Stability of electron-hole plasma in type-I and type-II GaAs-GaAlAs single quantum wells

Taro Ando*
Hamamatsu Photonics K.K., The 1st Research Group, Central Research Laboratory, Hirakuchi, Hamakita-City, Shizuoka 434-8601, Japan

Masaaki Nakayama and Makoto Hosoda
Department of Applied Physics, Graduate School of Engineering, Osaka City University, Sugimoto, Sumiyoshi-ku, Osaka 558-8585, Japan

(Received 26 November 2003; published 22 April 2004)

We calculate and compare energies of the electron-hole plasmas and ground-state excitons in type-I and type-II GaAs-GaAlAs single quantum wells with various structural conditions. Calculations are performed with a flexible and numerically stable method using realistic material parameters. We confirm that the exciton states are stable in type-I quantum wells for well widths up to 250 Å, as described in previous work [G. E. W. Bauer and T. Ando, Phys. Rev. B **34**, 1386 (1986)]. We find that the electron-hole plasma becomes stable, particularly in narrow type-II quantum wells, e.g., about 2.5 meV below the ground state exciton in GaAs-AlAs quantum wells whose widths are 6 and 4 monolayers, respectively. Moreover, calculations including electric fields reveal two different conditions of the stable electron-hole plasma: one is that electrons and holes are separated and the other is that they are confined in the narrow regions. The results suggest the possibility of observing the electron-hole plasma as the lowest excited state in the GaAs-GaAlAs quantum well.

DOI: 10.1103/PhysRevB.69.165316 PACS number(s): 73.21.Fg, 73.20.Mf, 71.35.Ee, 71.15.Nc

I. INTRODUCTION

The stability of the electron-hole plasma (EHP) compared to the ground state ($1s$) exciton in semiconductor two-dimensional (2D) structures has been a target of theoretical interest.[1–7] Experiments on EHP have also been performed extensively;[8–15] in particular, quantitative comparisons have been done between experimental results of luminescence spectra and theoretical calculations in type-I GaAs quantum wells (QW's).[8,9] Owing to these detailed studies, Refs. 7 and 8 provide us with the common conclusion that the EHP is unstable relative to the $1s$ exciton state in type-I GaAs-GaAlAs quasi-2D systems. However, there are no theoretical discussions on the stability of the EHP in type-II GaAs-GaAlAs systems, except in Ref. 7, while there are experimental observations of the EHP in type-II structures.[10–13]

In order to study the stability of the quasi-2D EHP and to clarify its mechanism, we calculate the total energies of the EHP and lowest $1s$ exciton, in this case, the $1s$ heavy-hole exciton, in type-I and type-II GaAs-GaAlAs single QW's. With the computational method presented in previous studies,[16,17] we can perform quantitative, numerically stable, and flexible EHP calculations under various conditions, e.g., QW structures, charge densities, and applied external electric fields. Moreover, a method is developed for calculations of excitons, including many-body effects of carriers. Our calculations are not exact ones for neglecting the effects of image charges and band nonparabolicity, but the estimated excitonic binding energies are in good agreement with previous works within a difference of ~ 1 meV.[18–20]

Results of calculations on type-I QW's show that the lowest 1s exciton states are stable up to a QW width of 250 Å [=90 monolayers (ML)], which is consistent with the conclusion in Ref. 8. Calculations are also performed on various structures of type-II GaAs-AlAs QW's with correct consideration of the anisotropic effective masses of electrons in the X state (X electron). Here, the structures are stacks of GaAs and AlAs layers whose widths are in the range of 4–10 ML and 4–35 ML, respectively, so that the X-electron states remain in the lowest conduction-band state. It is found that the EHP is stable in type-II QW's for heavy effective mass of the X electron, enhancing the effect of the exchange-correlation (XC) interaction, which is the only factor to stabilize the EHP. Additionally, we find that the EHP is stabilized by narrowing the wells in both type-I and type-II QW's because the concentration of the carriers into the narrow well also enhances XC interaction. However, the type-I EHP turns out to be unstable even though it is stabilized to its maximum.

Effects of external electric fields on the stability of EHP are also studied. By applying strong electric fields to QW's to separate electrons and holes, the binding energy of the $1s$ exciton can be reduced for spatial separation between the charges. Thus, the EHP is relatively stable compared to the exciton in this situation. Moreover, the type-II EHP is also found to become stable by applying the electric fields to merge electrons and holes. In this situation, the e-h pairs are gathered to strengthen the effect of the XC interaction, similar to the case of narrow QW's. We found that the difference between the energy of the merged EHP and the $1s$ exciton becomes about -2.5 meV, which also implies the stable formation of electron-hole liquid.

The outline of this paper is as follows. We describe the theoretical models for calculations in Sec. II. EHP and $1s$ excitons are formulated in Sec. II A and Sec. II B, respectively, and material parameters used in the calculations are listed in Sec. II C. In Sec. III, we present results of the calculations on the type-I and type-II GaAs QW's, as well as physical discussions of the results involving the effects of external electric fields. Finally, we summarize the results and discussions in Sec. IV.

II. THEORETICAL MODEL

A. Electron-hole plasma

1. Hamiltonian of the system

Here, we formulate the EHP in QW's grown in the z direction to calculate the properties of EHP. In the formulation, it is assumed that the electrons and holes occupy only the lowest subband levels of the conduction and valence bands, respectively, and that the total number of electrons and holes per unit area in the xy plane is equal and fixed to a constant value N_0. The Hamiltonian of the system per e-h pair is given as follows[21–25] as a functional of electron and hole wave functions [$\psi_e(z)$ and $\psi_h(z)$], which are supposed to be normalized:

$$E[\psi]=\sum_{\alpha=e,h}\int dz\,\psi_\alpha(z)\left[-\frac{\hbar^2}{2m_\alpha}\triangle+q_\alpha V_\alpha(z)\right]\psi_\alpha(z)+\frac{1}{2}\int dz\,\frac{\rho(z)}{\epsilon(z)}\int_{-\infty}^{z}dz'(z-z')\rho(z')+E^{\mathrm{XC}}, \quad (1)$$

where q_α is the charge on a carrier [the suffix $\alpha(=e,h)$ indicates an electron and a hole, respectively], z is a variable for the spatial position in the growth direction of quantum wells, and ϵ is an effective dielectric constant in media, which in general depends on the position. The total charge-density distribution $\rho(z)$ $[=N_0\Sigma_{\alpha=e,h}q_\alpha|\psi_\alpha(z)|^2]$ is introduced in the above expression for notational simplicity. In Eq. (1), m_α means the quantization effective mass of the carrier under consideration. Care is needed in the calculation of holes (the lowest heavy-hole state in this paper) and X electrons in type-II systems, because the quantization and parallel masses are different in the anisotropic states.

Equation (1) indicates that the Hamiltonian E consists of three terms: the kinetic and fixed potential-energy term, the Hartree interaction energy term, and the XC energy term, in order corresponding to the right-hand side of Eq. (1). The kinetic and fixed potential energy term is simply a quadratic form of the wave functions, i.e., the ''linear'' components of the total energy. It is also noted that the fixed potential $V_\alpha(z)$ is a sum of potentials due to the band edge and external electric field. On the other hand, the Hartree energy term represents the Coulomb interactions between electron-hole, electron-electron, and hole-hole that depend on the wave functions of carriers through the carrier density distributions. Finally, the XC energy term, which is a contribution of quantum many-body effects related to the fermionic nature of carriers, plays a significant role in the EHP. Further discussions are necessary to determine the explicit expression of the XC energy term.

2. Exchange-correlation energy

In this paper, we use an approximation for the XC energy to express as a sum of XC energies per electron and per hole in a single-component plasma, i.e.,

$$E^{\mathrm{XC}}=\int dz\{n_e(z)\varepsilon_e^{\mathrm{XC}}[n_e(z)]+n_h(z)\varepsilon_h^{\mathrm{XC}}[n_h(z)]\}, \quad (2)$$

where $\varepsilon_e^{\mathrm{XC}}$ and $\varepsilon_h^{\mathrm{XC}}$ are the XC energy densities for an electron and a hole, respectively. The XC energy densities are functionals of carrier density distributions $n_\alpha(z)$ $[=|\psi_\alpha(z)|^2]$. Here, we can use the XC energy density functional, which is often expressed by the following well-known formula according to the local-density approximation in the density-functional theory (DFT):[26–28]

$$\varepsilon^{\mathrm{XC}}(r_s)=\frac{e_0^4}{32\pi^2\hbar^2}\frac{m_\alpha^\perp}{\epsilon^2}\left(-\left(\frac{9\pi}{4}\right)^{1/3}\frac{3}{2\pi r_s}-0.0666\times\left\{\left[1+\left(\frac{r_s}{11.4}\right)^3\right]\ln\left(1+\frac{11.4}{r_s}\right)+\frac{1}{2}\frac{r_s}{11.4}-\left(\frac{r_s}{11.4}\right)^2-\frac{1}{3}\right\}\right), \quad (3)$$

where the first coefficient is the Rydberg factor for the conversion of energy units from rydbergs [Ry] to joules [J]. In the above expression, the density parameter r_s is an average distance between carriers scaled by the effective Bohr radius a_B in the medium,

$$a_B=\frac{4\pi\epsilon\hbar^2}{m_\alpha^\perp e_0^2}, \quad (4)$$

where e_0 denotes the elementary electric charge. When considering the position dependence of the dielectric constant and effective mass, a_B and r_s become functions of position z, thus, the XC energy density is finally reduced to a function of z.

The XC energy densities for an electron and a hole are defined with Eqs. (3) and (4) by substituting the effective masses of electrons and holes, respectively. Here, it is noted that the effective masses in Eqs. (3) and (4) relate to the estimation of the carrier density. Thus, by considering the symmetry, the effective mass should be chosen as that for the xy direction (i.e., parallel mass), especially when we study anisotropic states such as the heavy hole and X electron.[29]

The approximation of Eq. (2) for the XC energy is different from the Vashishta-Kalia approximation in Refs. 8 and 9, which is stated to be valid when the densities of electrons and holes are sufficiently similar. However, because of the need to study the type-II system where the electrons and holes are spatially separated, we use the approximation of Eq. (2). In the following section, it is shown that this approximation gives consistent results with Ref. 8 also in type-I systems.

3. Total energy and chemical potential

As a result of the minimization, the expectation value of the system's Hamiltonian (E) is also obtained together with the physical wave functions. The total energy of EHP is then calculated by adding the in-plane kinetic energy to E. Here, the in-plane kinetic energy is taken into account as the band-filling effects: when the total carrier number per unit area

(N_0) is given, the 2D density of state is defined as $m_\alpha^\perp/\pi\hbar^2$, and thus the chemical potential due to the in-plane motion (μ_α) becomes

$$\mu_\alpha = \frac{N_0 \pi \hbar^2}{m_\alpha^\perp}. \tag{5}$$

For average in-plane kinetic energy per carrier given as $\mu_\alpha/2$, the total EHP energy (E_{EHP}) finally becomes

$$E_{\mathrm{EHP}} = E + \frac{1}{2}(\mu_e + \mu_h). \tag{6}$$

We note that the effects of effective-mass mismatch in different materia are taken into account as the weighted spatial average ($\overline{m}_\alpha$) in the actual calculation. The definition of $\overline{m}_\alpha$ is given in the Appendix.

Another important quantity is the chemical potential, which is an energy necessary for adding one particle to the state under consideration and is defined by using the Kohn-Sham (KS) eigenvalues in DFT. The chemical potential is also needed for studying the formation of the electron-hole liquid.[7] By formally applying functional derivatives to the total Hamiltonian according to wave functions and setting the functional derivative to zero, we can obtain the corresponding effective one-particle Schrödinger equation, usually referred to as the KS equation:[26]

$$\left[-\frac{\hbar^2}{2m_\alpha}\Delta + q_\alpha V_\alpha(z) + q_\alpha V_\alpha^{\mathrm{H}}(z) + V_\alpha^{\mathrm{XC}}(z) \right] \psi_\alpha(z) = \mathcal{E}_\alpha \psi_\alpha(z), \tag{7}$$

where $V_\alpha(z)$ is a fixed electric potential term in Eq. (1) itself, i.e., a summation of a band-edge potential and a potential due to the external electric field. In addition, $V_\alpha^{\mathrm{H}}(z)$ and $V_\alpha^{\mathrm{XC}}(z)$ are a Hartree potential and an XC potential, respectively. It is also noted that $\mathcal{E}_\alpha$ is a KS eigenvalue, i.e., an energy eigenvalue of the effective one-particle Schrödinger equation for state α. The Hartree potential is defined as a functional derivative of the Hartree energy term (Eg^{H}),

$$q_\alpha V_\alpha^{\mathrm{H}}(z) = \frac{\delta E^{\mathrm{H}}}{\delta n_\alpha(z)} = \frac{q_\alpha}{\epsilon(z)} \int_{-\infty}^{z} dz'(z-z')\rho(z'), \tag{8}$$

which actually corresponds to a potential of charge sheets on an infinite plane. Similarly, the XC potential is defined as

$$V_\alpha^{\mathrm{XC}}(z) = \frac{\delta E^{\mathrm{XC}}}{\delta n_\alpha(z)} = \varepsilon_\alpha^{\mathrm{XC}}[n_\alpha(z)] + n_\alpha(z)\frac{d\varepsilon_\alpha^{\mathrm{XC}}(n_\alpha)}{dn_\alpha}, \tag{9}$$

whose explicit form is obtained by substituting Eq. (3) into the above expression. Now, the total chemical potential (μ_{EHP}) of the EHP system is finally defined as

$$\mu_{\mathrm{EHP}} = \mathcal{E}_e + \mathcal{E}_h + \mu_e + \mu_h. \tag{10}$$

It is noted that $\mathcal{E}_e + \mathcal{E}_h$ gives a ''band gap'' shrunk by the XC interaction.

Because the discussion on the stability of EHP depends on the small difference between the energies of the exciton and EHP while the energies themselves are large values, small corrections on subband levels appear to be relevant to the stability of the EHP. In this sense, a small effect such as the complex valence-band structure[30] appears to modify the relative difference between those two energies. Nevertheless, we can estimate the band-mixing effect on the filling phenomena of hole subbands to be ignorable for the following reason: the band-mixing effect appears significantly in the large N_0 region where the Fermi level of the hole is closed to higher valence-band levels. However, the EHP becomes most stable in the relatively small N_0 region, where the Fermi level of the hole state is at most a few meV higher from the bottom of the lowest valence-band state, as shown in a later section. (This is also true for the exciton, because the minimum energy of the exciton is achieved in the limit of $N_0 \to 0$.) Therefore, we can validate our model to neglect the band-mixing effect.

We can easily develop a procedure for the practical numerical computations from the above formulations. The essence of the numerical procedure is the discretization of wave functions based on the finite-differential approach. Once the wave functions are discretized to a set of values on the discrete points in the z direction, the Hamiltonian functional [Eq. (1)] is reduced to an ordinal multivariate function of components of the discretized wave functions. This approach has the virtue that the physical states are obtained by applying a nonlinear minimization procedure, for example, the conjugate gradient method, to the total energy even if the total energy includes nonlinear interactions. Moreover, in the practical calculation, position-dependent parameters are taken into account, such as the effective mass and dielectric mismatch in the different materia. Details of the calculation method are described in Refs. 16 and 17.

B. Ground-state exciton

There are many studies on the calculation of exciton binding energies in GaAs QW's.[18–20,31–34] Here, we adopt the variational approach in Refs. 31 and 33, which is one of the simplest; nevertheless, it effectively represents the ground-state properties of the system under consideration.

In general, the total exciton wave function is expressed approximately as

$$\Psi(r, z_e, z_h) = \psi_e(z_e)\psi_h(z_h)\phi_{e\text{-}h}(r, z_e - z_h) \tag{11}$$

in the variational formalism, where z_e and z_h are the position of the electron and hole in the z direction, respectively. In Eq. (11), $\phi_{e\text{-}h}$ represents the relative motion between the electron and hole and is referred to as an envelope function of the exciton. As our purpose is to study the ground-state properties of 2D QW's, only the lowest exciton state, i.e., the $1s$ state, is considered in the following. Based on this assumption, the trial envelope function can be chosen as the following form with variational parameters ζ and λ:

$$\phi_{e\text{-}h}(r, z_e - z_h) = \exp\left[-\frac{\sqrt{r^2 + \zeta^2 (z_e - z_h)^2}}{\lambda} \right], \tag{12}$$

where $r^2=x^2+y^2$, for angular momentum in the 2D space of the 1*s* exciton is zero. According to Ref. 33, the trial function Eq. (12) agrees well with the true exciton envelope function. The total Hamiltonian of the exciton is also defined as :

$$\hat{H}_{\mathrm{EXC}}=\hat{H}_e+\hat{H}_h+\hat{H}_{e\text{-}h} \quad , \tag{13}$$

where $\hat{H}_e$ and $\hat{H}_h$ are the one-particle Hamiltonians for the electron and hole, respectively, i.e.,

$$\hat{H}_{e,h}=-\frac{\hbar^2}{2m_{e,h}}\frac{\partial^2}{\partial z_{e,h}^2}+V_{e,h}(z_{e,h}), \tag{14}$$

and $\hat{H}_{e\text{-}h}$ is the Hamiltonian corresponding to the relative motion between the electron and hole, i.e.,

$$\hat{H}_{e\text{-}h}=-\frac{\hbar^2}{2M^{\perp}}\left(\frac{\partial^2}{\partial x^2}+\frac{\partial^2}{\partial y^2}\right)-\frac{e_0^2}{4\pi\epsilon\sqrt{r^2+(z_e-z_h)^2}}. \tag{15}$$

In the above expression, $M^{\perp}$ is a reduced in-plane effective mass, i.e., $1/M^{\perp}=1/m_e^{\perp}+1/m_h^{\perp}$. The expectation value of the Hamiltonian $\langle\hat{H}_{\mathrm{EXC}}\rangle$ is obtained by using Eqs. (12) and (13), considering the operator action of the Hamiltonian on the wave functions. Following the derivation in Refs. 31 and 33, $\langle\hat{H}_{\mathrm{EXC}}\rangle$ becomes

$$\langle\hat{H}_{\mathrm{EXC}}\rangle=(E_e+E_h)+\frac{\hbar^2}{2M^{\perp}}\int dap(a)[G(a)-J(a)] - \frac{e_0^2}{4\pi\epsilon}\int dap(a)K(a), \tag{16}$$

where $E_{e,h}$ represents the energies of electrons and holes, respectively, and $p(a)$ is the uncorrelated probability of finding an electron and a hole separated by a distance a in the z direction:

$$p(a)=\int dz[|\psi_e(z+a)|^2|\psi_h(z)|^2+|\psi_e(z)|^2|\psi_h(z+a)|^2]. \tag{17}$$

Moreover, $G(a)$, $J(a)$, and $K(a)$ relate to the relative z motion, xy motion, and Coulomb interaction, respectively. The explicit expressions of $G(a)$, $J(a)$, and $K(a)$ are given in the Appendix. Equation (16) denotes that the exciton total energy consists of subband energy, relative kinetic energy, and potential energy. Among these three components, a summation of relative kinetic and potential energy gives an exciton binding energy, which is always negative for the bound state.

Usually, the Hartree interaction is neglected when calculating the exciton binding energy, but it has significant effects, especially in type-II systems, because the charge screening does not sufficiently work for the spatial separation between the opposite charges. In this study, the effects of the Hartree interaction are taken into account as changes of subband energies of the electrons and holes ($E_{e,h}$). This means that excitons are formed by the electrons and holes in the subband states under mean electric fields from other carriers. Strictly speaking, the envelope function actually influences the electron and hole subband, thus the exciton states should be determined self-consistently.[31–33] However, these effects are less than 1 meV and can be neglected compared to other significant contributions.

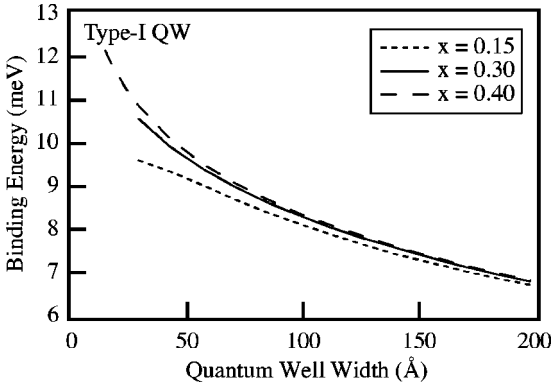

FIG. 1. Binding energies of 1*s* excitons in type-I GaAs QW's calculated with the present method. The calculations are performed for different alloy ratios of Al compound ($x=0.15$, 0.30, and 0.40) in $Ga_{1-x}Al_xAs$ barriers. For comparison to previous studies (Refs. 18–20), the signature of the binding energy is reverted.

For the bosonic nature of the exciton, the statistical effects can be neglected, especially in the small density region where the exciton energy reaches a minimum. Additionally, calculation of the minimum exciton energy without XC interaction gives reliable values, for the Gunnardson-Lundqvist formula, Eq. (3), becomes inaccurate in the low-density limit.[27] Thus, the exciton energy is calculated without the XC interaction in this paper.

In summary, the procedure to calculate the 1*s* exciton energy becomes the following:

Step. 1 Calculate the electron and hole subband energies according to the method in Sec. II A without the XC interaction term.

Step. 2 Apply the nonlinear minimization procedure to $\langle\hat{H}_{\mathrm{EXC}}\rangle$. In this step, $\psi_{e,h}$ are fixed to those obtained in the previous step and the minimization is performed on the variational parameters (ζ and λ).

Step. 3 Calculate the total energy of the exciton by using the variational parameters determined in the previous step.

In the actual calculations, the variational parameters are scaled or reparametrized to improve the stability of the minimization procedure.

Figure 1 shows binding energies of 1*s* excitons as a function of the width of type-I QW's obtained with the present method. The results show good agreement with other works within a difference of $\sim$1 meV.[18–20] Results in Fig. 1 show somewhat smaller values than those in Ref. 34 because the effects of image charges are not considered in our model. Because of the neglect of the image charge effect, the present calculation seems to have difficulty calculating the absolute energy values; nevertheless, it is still effective for the relative comparison between EHP and the exciton by neglecting the image charge effect commonly in the calculation of EHP and

TABLE I. Material parameters used in the calculations. The effective masses are given in the unit of the electron mass in free space (m_0) and the dielectric constants are in the unit of the dielectric constant in vacuum (ϵ_0). Heavy-hole effective masses are calculated by using the Luttinger parameters (Ref. 42) ($\gamma_1^{\mathrm{GaAs}}=6.85, \gamma_2^{\mathrm{GaAs}}=2.10$, $\gamma_1^{\mathrm{AlAs}}=3.45$, and $\gamma_2^{\mathrm{AlAs}}=0.68$) and interpolated according to the alloy ratio of $Al_xGa_{1-x}As$.

	Values in $Ga_{1-x}Al_xAs$
m_Γ	$0.067+0.083x$[a]
m_X	$1.30-0.2x$[b]
$m_X^\perp$	$0.23-0.04x$[c]
m_h	$0.377+0.101x$
$m_h^\perp$	$0.112+0.129x$
ϵ	$12.53-2.47x$
ΔV_Γ (eV)	$1.424+1.594x+(1.310x-0.127)x(x-1)$[d]
ΔV_X (eV)	$1.900+0.125x+0.143x^2$[e]

[a]Reference 36.
[b]References 37 and 38.
[c]References 38 and 39.
[d]Reference 40.
[e]Reference 41.

1*s* excitons. Additionally, the calculated binding energies of type-II excitons are also in good agreement with the results in type-II QW's.[35] Therefore, we can conclude that the present method gives reliable values for exciton binding energies.

C. Material parameters

It is important to clarify the parameters in calculations because the choice of material parameters has significant effect on the EHP and 1*s* exciton binding energy to the order of a few meV. Table I summarizes the material parameters used in the computations. In the table, ΔV_Γ is the direct gap between the Γ_8 valence and Γ_6 conduction bands,[40] whereas ΔV_X is the indirect gap between the Γ_8 valence and X_6 conduction band.[41] The effective masses and dielectric constants are linearly interpolated between those in GaAs and AlAs to take the material dependency into account.[42] It is also noted that the conduction and valence-band offsets are chosen as 0.67 and 0.33, respectively.

III. RESULTS AND DISCUSSIONS

The EHP and 1*s* exciton energies are given as functions of the *e-h* pair density (N_0). To discuss the stability of EHP according to the 1*s* exciton, the minimum energies of the EHP and 1*s* exciton per *e-h* pair are calculated and compared in various conditions, e.g., QW structures and external electric fields, in this section. In the following discussion, E_{EHP} and E_{EXC} are used to indicate the minimum values of E_{EHP} and 1*s* exciton energies, respectively. For all calculations in this study, the division number of the *z* direction is fixed to 20 points/ML, which is a sufficiently fine division for the purpose of this study.

A. Type-I quantum well

Electron and hole wave functions obtained in the EHP calculations are shown in Fig. 2, which help with the physical interpretation of calculation results. In Figs. 2(a)–2(c), wave functions at N_0 for the minimum EHP energy are displayed, while in Fig. 2(d), wave functions in high-density EHP are shown, although the EHP is not stable at that density. Furthermore, it is noted that the assumption of single subband occupation is reasonable around the minimum EHP energy conditions. This is because the chemical potentials (dotted lines) in Figs. 2(a)–2(c) are close to the lowest subband levels, indicating that carriers cannot occupy the upper states. In addition, Figs. 3(a) and 3(b) show typical results for the EHP and 1*s* exciton energies in 50 ML GaAs QW surrounded by $Ga_{0.56}Al_{0.44}As$ (40 ML) barriers with and without electric fields, respectively. It is noted that Fig. 3(a) corresponds to previous studies.[7,8]

To begin with, we review characteristics of the Hartree and XC interactions. In the EHP system, the XC interaction, whose contribution is always negative, is the only factor to stabilize the EHP. Here, the XC energy itself depends weakly on N_0 and does not change greatly due to a local change of charge distributions unless the deformation of wave functions is so large that the peaks of the charge distributions vary by more than an order with the same N_0. We can, therefore, estimate the XC interaction equally in both flat-band and weakly biased conditions. Contrarily, the Hartree interaction term is always positive [Eq. (1)] and becomes zero only when the electron and hole distributions are strictly the same. Hence, when electric fields are applied, the Hartree energy increases as the difference between electron and hole distributions also increases as N_0 becomes larger, even if the charge neutrality is totally satisfied.

By considering these characteristics of the Hartree and XC interactions, the behavior of the band gaps in Figs. 3(a) and 3(b) can be explained. In the flat-band condition [Fig. 3(a)], the charge screening effect cancels the Hartree interaction, hence band-gap shrinkage due to the XC interaction is clearly observed in large N_0 regions. On the other hand, when biased with the electric fields, the unscreened Hartree interaction produces a significant contribution. In this case, the Hartree energy, which depends quadratically on N_0, easily overcomes the weak dependency of the XC energy on N_0. Consequently, the band gap starts to increase around $N_0 \sim 10^{10}/\mathrm{cm}^2$ in Fig. 3(b). However, if N_0 is further increased, the external electric field can be canceled with small deformations of the charge distributions, so the wave functions retrieve the symmetry as shown in Fig. 2(d). In these regions, the system behaves similarly to the unbiased type-I QW and the band gap starts to shrink for each increment of N_0.

Based on the behavior of the band gap, we can discuss the formation of EHP. In the flat-band type-I QW, the band gap shrinks due to the XC interaction the larger N_0 becomes. At the same time, the kinetic energy of the in-plane motion increases, i.e., the chemical potential due to the in-plane motion ($\mu_\perp = \mu_e + \mu_h$) increases monotonically in proportion to N_0. Thus, the total chemical potential of EHP has a mini-

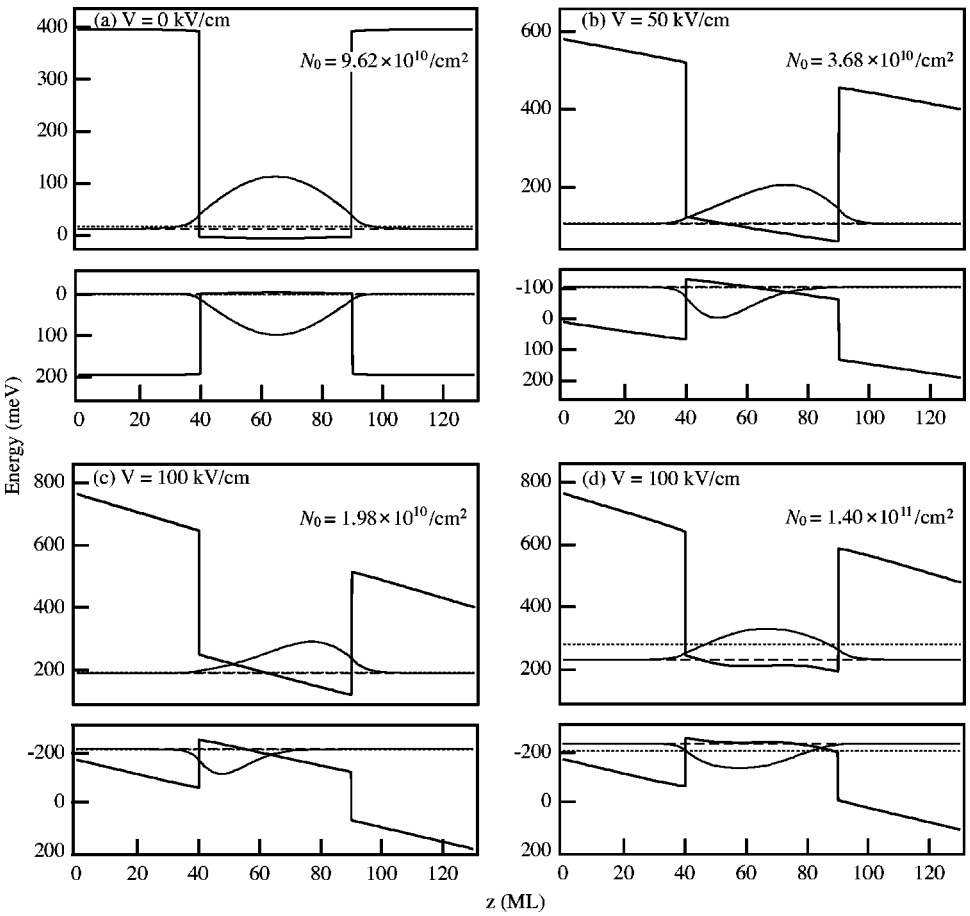

FIG. 2. Electron and hole wave functions (solid curves) in GaAs (50 ML) QW's with $Ga_{0.56}Al_{0.44}As$ (40 ML) barriers. The upper part of each figure shows the conduction-band profile while the lower part shows the valence-band profile. (a) Flat-band condition, (b) with electric field of 50 kV/cm, (c) with electric field of 100 kV/cm, and (d) with the same bias condition as (c) but higher *e-h* pair density ($N_{e\text{-}h} = 1.7\times10^{11}$ /cm^2). $N_{e\text{-}h}$ in (a)–(c) are chosen so that they give the minimum EHP energies. It is noted that dashed lines and dotted lines indicate the subband levels and chemical potentials, respectively, although they appear to be single lines in (a)–(c) because the chemical potentials are so close to the subband levels.

mum due to the competition between the XC potential and in-plane motion. The EHP energy also behaves similarly to the chemical potential, as shown in Fig. 3(a), because the energy and KS eigenvalue of the XC (and Hartree) term differ at most by a factor. In the case of a biased situation, the Hartree interaction pushes up the band gap without accounting for the in-plane kinetic energy. After all, the minimum of EHP energy must be realized at a smaller $\mu_\perp$, i.e., a smaller N_0 than in the flat-band situation. In fact, the decrease of N_0 for the minimum EHP energy by the electric field is observed in Figs. 2(a)–2(c).

Another important fact in Fig. 3(b) is that E_{EXC} is minimized in the small N_0 limit where the band bending due to the carrier concentration in the quantization direction (i.e., z direction) does not occur. This is always true in every condition, which is consistent with the positive-definite nature of the Hartree interaction. Thus, when analyzing the behavior of the minimum exciton energies, the relative motion between the electron and hole plays the principle role.

It is also noted that the approximation of Eq. (2) ignores the electron-hole correlation. The electron-hole correlation becomes countable in type-I QW's rather than in type-II QW's, because the spatial overlap of the electron and hole is too small to produce the significant electron-hole correlation in the type-II QW's. However, we can estimate the effect to be sufficiently small in type-I QW's by comparing Fig. 3(a) to the result in Ref. 8, which is obtained with consideration of the electron-hole correlation. Thus, the discussion in this paper is valid at least semiquantitatively.

1. Effects of quantum well width

Figure 4 shows energies of the EHP and 1*s* excitons in type-I GaAs QW's of different widths without external electric fields. The difference between the energies of the EHP and 1*s* exciton ΔE ($=E_{\mathrm{EHP}}-E_{\mathrm{EXC}}$) is also shown in this figure. The behavior of ΔE is explained in different ways for wide and narrow QW's. In wide QW's, the kinetic energy is so low that the Hartree and XC interactions significantly affect the electron and hole wave functions. This leads to the wave functions being determined mainly to minimize the interaction energies, so the Hartree energy is small for charge cancellation and becomes insensitive to the QW width. Moreover, the XC energy changes little with the QW width (particularly in wide QW's), for the XC interaction depends weakly on the density. However, the binding energy of the 1*s* exciton decreases significantly as the QW becomes wider, even for widths of over 50 ML (Fig. 1). As a result, ΔE is slightly reduced in wide QW regions.

On the other hand, the kinetic energy associated with the motion in the z direction is so large in the narrow QW that the wave functions are determined mainly to reduce it. Hence, we can suppose that the Hartree interaction is not sufficiently screened and that the EHP is destabilized by the unscreened Hartree interaction. Here, for there is no anoma-

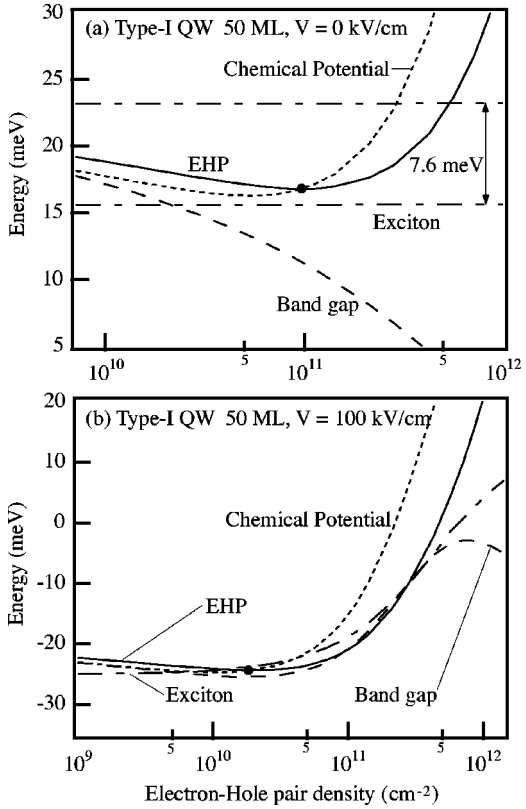

FIG. 3. Energies of EHP (solid line) and 1*s* exciton (dash-dotted line) with band gaps (dashed line) and chemical potentials (dotted line) in type-I GaAs (50 ML) QW surrounded by $Ga_{0.56}Al_{0.44}As$ (40 ML) barriers as functions of the *e-h* pair density. (a) Flat-band condition and (b) biased with the electric field of 100 kV/cm. It is noted that the band gap of bulk GaAs (1.424 eV) must be added to each value for discussion of the luminescent band. The closed circle shows the realization of the electron-hole liquid, where the chemical potential becomes equal to the EHP energy (Ref. 7).

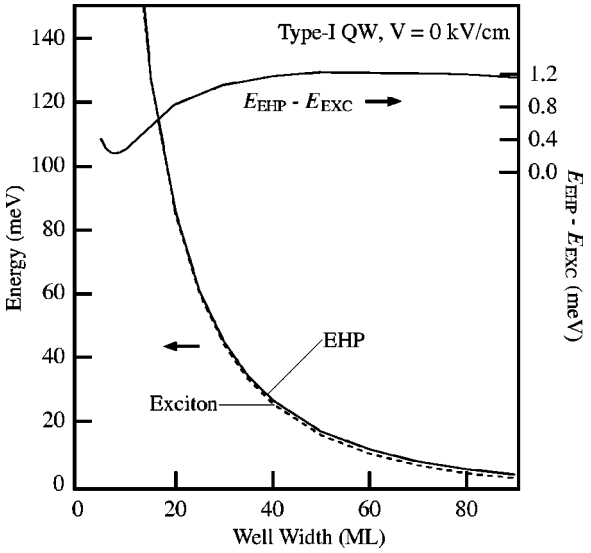

FIG. 4. The minimum energies of EHP (solid line) and 1*s* exciton (dotted line) for various well widths of type-I QW's (GaAs QW's with 40 ML $Ga_{0.56}Al_{0.44}As$ barriers). The difference between the two energies ($E_{EHP}-E_{EXC}$) is also shown to reveal small differences. Note that the *e-h* pair densities to realize the minimum EHP energies are in the range of $10^{10}/cm^2$–10^{11} $/cm^2$, while the minimum 1*s* exciton energies are always realized in the low-density limit.

lous behavior of the exciton binding energy in narrow QW's (Fig. 1), we can reach the conclusion that ΔE increases as the QW width is reduced. However, this perspective actually conflicts with the observation that ΔE markedly decreases around the QW thickness of 10 ML. It is difficult to give a quantitative picture of the behavior because the EHP in the narrow QW is realized as the result of the subtle competition among the quantum confinement effect, Hartree interaction, XC interaction, and filling effect due to the in-plane kinetic energy. Nevertheless, by analyzing the EHP energy in detail, we find that the XC energy is dominant (-15.2–17.5 meV), while the Hartree energy changes by finite but negligible amounts (0.03–0.07 meV), and the chemical potential due to the in-plane motion also changes little. Therefore, the behavior of ΔE around a well width of 10 ML is phenomenologically assigned to the enhanced XC interaction due to the carrier concentration within the narrow QW. When the QW width is further reduced, the exciton binding energy increases while the Hartree and XC energies do not change significantly, resulting in the relative increase of ΔE. The behavior of ΔE in narrow QW's is also discussed in Sec. III B 1.

In any case, the result that the ΔE is always positive in Fig. 4 means that excitons are always stable in type-I QW's. There still remains the possibility of a stable EHP in wide QW's; however, the QW picture becomes meaningless in well widths above 100 ML, and the situation is outside the interest of this study. Thus, we can conclude that the EHP is not stable in flat-band type-I QW's.

2. Effects of electric field

Figure 5 shows the effects of electric fields on the EHP and 1*s* exciton energies. A 50 ML QW width is chosen for clearly observing the effects of the electric field. Because the QW is not too narrow, we can explain the behavior of ΔE in Fig. 5 with a discussion similar to that given at the beginning of this section.

The global decrease of ΔE is caused mainly by the decrease of exciton binding energies for separation of electrons and holes due to the electric field. On the other hand, around the weak electric field, the increase of EHP energy is explained as the increase in the Hartree energy due to the charge separation. In fact, the Hartree/XC energies are 12 μeV/-10.28 meV, 0.7298 meV/-9.759 meV, and 2.440 meV/-8.444 meV for electric fields of 0, 20, and 40 kV/cm, respectively, in agreement with the physical picture.

It is expected that stronger electric fields on wider QW's can achieve a stable type-I EHP. Actually, calculation on a 90 ML QW under an electric field of 120 kV/cm results in $E_{EHP}-E_{EXC}=-3$ meV. However, the EHP will not produce luminescence because of a large *e-h* separation, and it is not physically interesting as quasi-2D states.

After all, the quasi-2D EHP is less stable than the 1*s* exciton in type-I GaAs QW's, regardless of whether the ex-

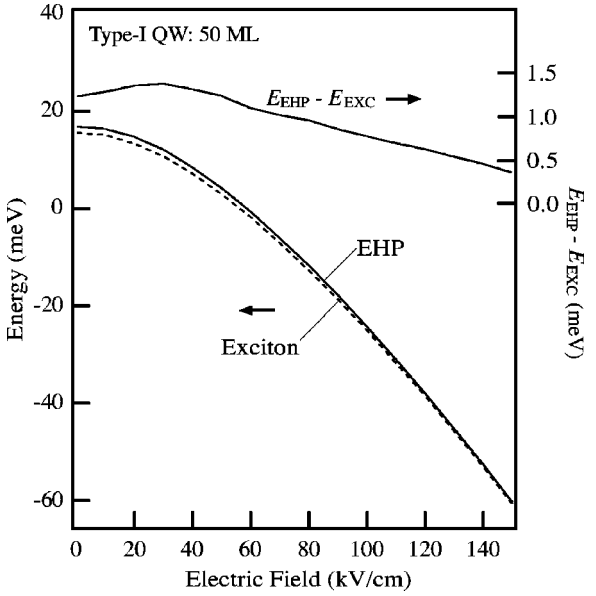

FIG. 5. The minimum energies of EHP (solid line) and 1*s* exciton (dotted line) in type-I QW's (50 ML GaAs QW's with 40 ML $Ga_{0.56}Al_{0.44}As$ barriers) as functions of electric fields. The difference of both energies ($\Delta E = E_{EHP} - E_{EXC}$) is also shown to reveal small differences. It is noted that the electric fields above 150 kV/cm cause tunneling of carriers out to the QW's.

ternal electric fields are applied. The main reason for the unstable EHP is possibly the small effective mass of Γ electrons, which also reduces the effects of the electric fields.

B. Type-II quantum wells

Here, we investigate the stability of EHP in type-II GaAs-AlAs QW's, where the lowest electron state is the *X* state in the AlAs layer. We focus our attention on the stability of the EHP according to the structural conditions of the type-II QW's and electric fields. Calculations are performed on GaAs-AlAs type-II single QW's, which are sandwiched between 40 ML $Ga_{0.56}Al_{0.44}As$ barriers.

As examples of EHP calculations, wave functions and band-edge profiles under typical type-II conditions are shown in Fig. 6 for supporting the physical picture. Results of the type-II EHP and 1*s* exciton energies as functions of N_0 are also shown in Figs. 7(a) and 7(b). Chemical potentials and band gaps are also shown in the figures, which present similar behavior to those in Ref. 7. In Fig. 7(a), the band gap starts to increase in the high-density region, which is assigned to the effects of Hartree interaction as in the previous discussion in Sec. III A. A result in a biased condition is also shown in Fig. 7(b), which shows similar behavior to

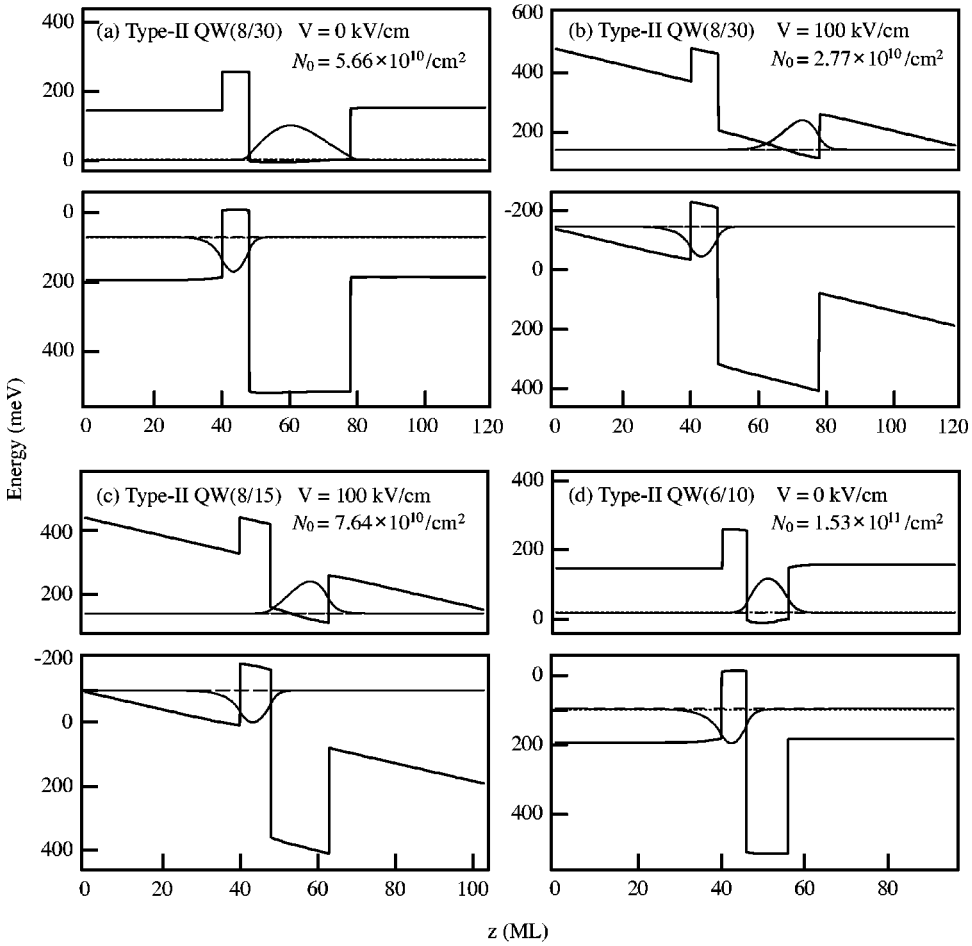

FIG. 6. Typical electron and hole wave functions (solid curves) in type-II GaAs-GaAlAs QW's. The upper part of each figure shows the conduction-band profile while the lower part shows the valence-band profile. It is noted that the conduction-band profiles are those for the *X* electron. (a) GaAs(8 ML)-AlAs(30 ML), flat-band condition; (b) GaAs(8 ML)-AlAs(30 ML) with external electric field of 100 kV/cm; (c) GaAs(8 ML)-AlAs(15 ML) with external electric field of 100 kV/cm; and (d): GaAs(6 ML)-AlAs(8 ML), flat-band condition. All figures are at *e*-*h* densities where the EHP energies are minimized. As in Fig. 2, subband levels and chemical potentials are indicated as dashed lines and dotted lines, respectively; however, they appear to be single dashed lines, which means that the subband filling effect is small at N_0 for the minimum EHP energy.

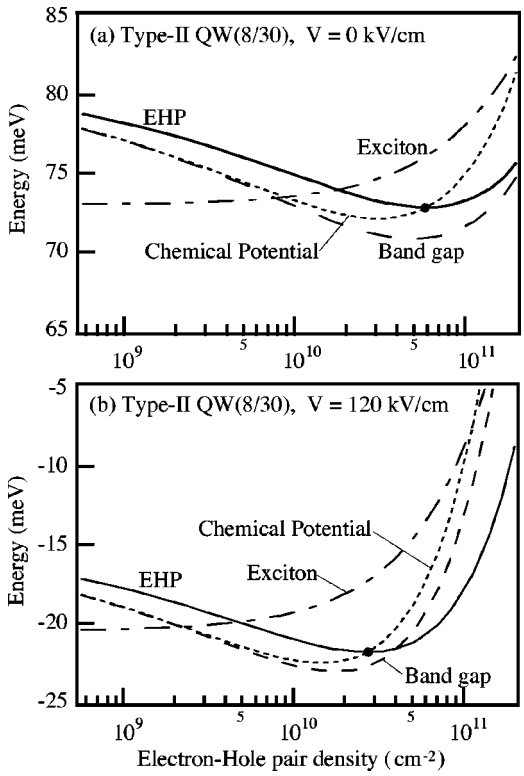

FIG. 7. The minimum energies of EHP (solid line) and 1*s* exciton (dash-dotted line) for various electron-hole pair densities in typical type-II GaAs(8 ML)-AlAs(30 ML) QW's with $Ga_{0.56}As_{0.44}As$ barriers: (a) flat-band condition and (b) with external electric field of 120 kV/cm. Chemical potentials and band gaps are also denoted as dotted and dashed lines, respectively. The intrinsic band gap between the heavy hole in GaAs and the *X* electron in AlAs (1.642 eV) must be added to each value for discussion of the luminescent band. The closed circle shows the energy of the electron-hole liquid as in Fig. 3.

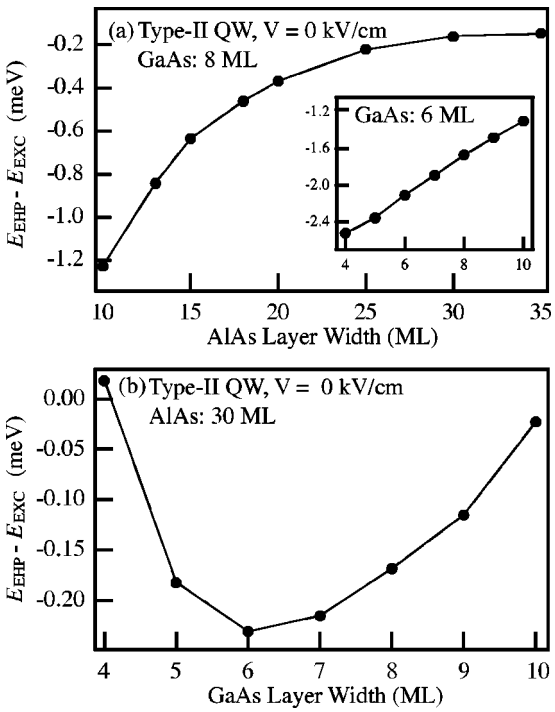

FIG. 8. Variation of the difference between the minimum EHP and 1*s* exciton energies ($\Delta E = E_{EHP} - E_{EXC}$) according to the QW width in type-II QW's with 40 ML $Ga_{0.56}Al_{0.44}As$ barriers. (a) ΔE for various widths of the AlAs layer with the GaAs layer fixed at 8 ML; the inset shows the results for AlAs layers of less than 10 ML with 6 ML GaAs layers, and (b) ΔE for various widths of the GaAs layer with the AlAs layer fixed at 30 ML.

Fig. 7(a), except that the electric field improves the stability of EHP. The effect of the electric fields is discussed in the following section.

In our calculations, the energy of a type-II 1*s* exciton is increased according to N_0 as shown in Fig. 7, which is consistent with the behavior of the Hartree energy in large N_0 regions.[43] It is also noted that the total binding energy of the exciton is not as small in type-II QW's as expected because the Hartree interaction is small for the separation between *e-h* pairs. However, the kinetic energy of relative motion is also reduced due to the large effective mass of *X* electrons.[35] For example, the binding energy of the type-II exciton in a GaAs(8 ML)-AlAs(30 ML) QW is typically -9.391 meV, which is the sum of the kinetic (4.233 meV) and potential (-13.624 meV) energies. On the other hand, the type-I exciton in a GaAs(22 ML) QW has a similar binding energy of -9.353 meV; however, the kinetic (6.75 meV) and potential (-16.103 meV) energies are very different from those of the type-II exciton.

1. Effects of quantum well structures

The stability of the type-II EHP is studied as a function of the QW width in Fig. 8 under the flat-band condition. In Fig. 8(a), the difference between the energies of EHP and the 1*s* exciton, ΔE, is shown for various widths of the AlAs layer, where the electrons are confined. ΔE is also shown in Fig. 8(b) by changing the widths of the GaAs layer. In Fig. 8(a), calculation results are shown for AlAs widths of over 10 ML because the *X*-electron states in narrow AlAs layers of less than 10 ML exceed the Γ-electron state in the 8 ML GaAs layer and the system changes into type I. To investigate the stability of the EHP in narrow type-II QW's, calculation results in the narrow AlAs layers of less than 10 ML with the 6-ML GaAs layer are shown in the inset in Fig. 8(a).

In Fig. 8(a), we can observe that the EHP is stable in the type-II GaAs-AlAs QW's and that the stability is enhanced by narrowing the AlAs layer. According to the discussion in Sec. III A 1, the enhanced stability is mainly due to the increase in XC energy due to the condensation of the carriers in the narrow region. Indeed, the concentration of carriers according to the widths of QW's is observed in Fig. 7.

Figure 8(b) also shows that the EHP is stabilized by reducing the widths of the GaAs layer from 10 ML to 6 ML. The change of ΔE is smaller than that in Fig. 8(a) because the hole in the GaAs layer is already concentrated sufficiently at a width of 10 ML and the effect of narrowing the GaAs layer is saturated. Thus, the inset of Fig. 8(a), showing the results in the 6-ML GaAs layer, presents the possibility of the most stable EHP in the GaAs-AlAs type-II QW's, which lies about -2.5 meV below the 1*s* exciton state.

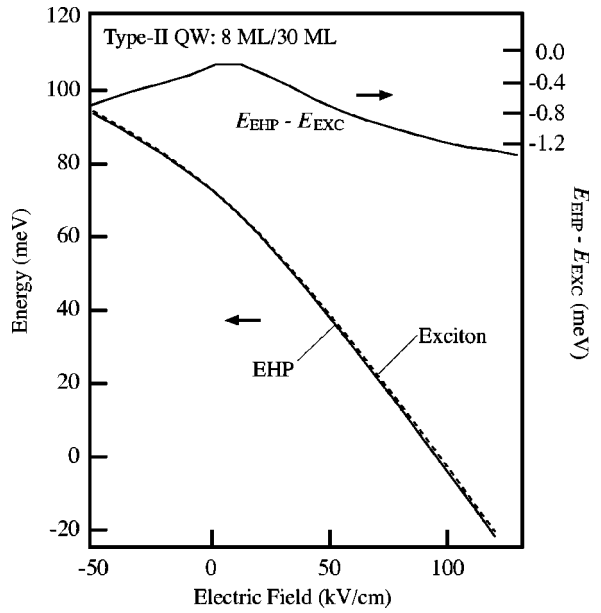

FIG. 9. The minimum energies of electron-hole plasma (solid line) and 1*s* exciton (dotted line) for various strengths of the external electric fields in type-II QW's [GaAs(8 ML)-AlAs(30 ML) QW's surrounded by $Ga_{0.56}Al_{0.44}As$ (40 ML) barriers]. The difference of the energies ($\Delta E = E_{EHP} - E_{EXC}$) is also shown to reveal small differences. Negative electric fields mean the direction to merge electrons and holes, while positive fields mean the direction to separate them.

However, the EHP becomes unstable when the width of the GaAs layer is reduced to less than 6 ML, which is similarly observed in the narrow type-I QW's (Sec. III A 1). The analysis of the EHP energy reveals that the Hartree and XC energies are saturated and increase the energy of the EHP only by small amounts as the GaAs layer narrows from 6 ML to 4 ML: the XC energy increases by about 0.1 meV, while the Hartree energy decreases by about 0.05 meV, the sum of which does not match the change in Fig. 8(b). Nevertheless, the binding energy of the 1*s* exciton increases significantly, supplementing the stability of the exciton. The saturation of the Hartree and XC energies is physically explained as that the hole wave function does not concentrate further by narrowing of the GaAs QW's below 6 ML. This explanation can be applied to the case of narrow type-I QW's, but it should be noted that the Γ electron mainly suffers from the effect of the narrowing in type-I QW's. Here, the subband level of the Γ electron is pushed up easily because of its small effective mass compared to the heavy hole, hence the type-I exciton is stabilized in a somewhat wider QW ($\sim$8 ML) than the type-II exciton, as seen in Fig. 4.

2. Effects of external electric fields

Figure 9 shows the effects of the electric field on the EHP and 1*s* exciton in type-II GaAs(8 ML)-AlAs(30 ML) QW's. The signature of the electric field is defined so that the positive electric field is directed to separate the electrons and holes. The width of the AlAs layer is chosen as 30 ML in order to study the effect of the electric field, because the effect is too small to be observed clearly in AlAs layers of less than 15 ML.

The behavior of ΔE is similar to that in type-I QW's (Fig. 5): the EHP is stabilized under strongly positive electric fields due to the reduction of the excitonic binding energy, and also stabilized under negative electric fields due to the enhancement of the XC interaction and suppression of the Hartree interaction.

To summarize, calculation results on the energies of the EHP and 1*s* exciton in type-I and type-II QW's have been shown and discussed in this section. It is noted that ΔEs showed similar behavior in type-I and type-II QW's, but that the amounts were very different. The difference was assigned to the effective masses of the Γ and *X* electrons in type-I and type-II QW's, respectively: the effects of the effective mass appear in the Rydberg factor and density parameter r_s in Eq. (3). When the effective mass becomes large, these effects commonly enhance the XC interaction to reduce the total EHP energy. Additionally, the large effective mass reduces the chemical potential due to the in-plane kinetic motion, which also stabilizes the EHP.

From the discussion in this section, we have found that the quasi-2D EHP is stabilized by separating the electrons and holes distantly to reduce the excitonic binding energy, and by confining them to the narrow region to enhance the XC interaction. In particular, we showed the EHP lying below the 1*s* exciton by more than 2.5 meV in the negatively biased narrow type-II QW. This also implies the EHP is possibly more stable than the biexciton, whose energy per *e-h* pair is smaller than that of the 1*s* exciton by at most a few meV,[44] although more detailed calculations are needed to confirm this.

We note that the minimum energy of the EHP is always close to the energy of the electron-hole liquid, as observed in Figs. 3 and 7 (indicated as closed circles in both figures), and hence that the above discussions on the EHP are also effective in the electron-hole liquid. Moreover, considering that the radiative lifetime of the type-II EHP luminescence is long thanks to the indirect nature of the type-II transition, we can expect the formation of electron-hole droplets in type-II GaAs-AlAs QW's.

IV. SUMMARY AND CONCLUSION

In this work, we developed a numerically stable method based on the quantum-mechanical variational principle with nonlinear interactions and performed quantitative calculations on the EHP and 1*s* exciton in type-I and type-II GaAs-GaAlAs single QW's in order to study the stability and mechanism of the EHP. By comparing the energy of the EHP and 1*s* exciton in various conditions of QW structures and electric fields, we found that the quasi-2D EHP is not stable in type-I GaAs QW's, but that the EHP becomes stable compared to the 1*s* exciton in type-II GaAs-AlAs QW's. We also found that a stable EHP is realized in two situations; when the electron and hole are separated, thus the excitonic binding energy is small, and when the electrons and holes are confined in the narrow QW's so that the XC interaction

works dominantly to stabilize the EHP. The estimated maximum stability of the EHP according to the 1*s* exciton is at least -2.5 meV per *e-h* pair, suggesting the possibility that the EHP becomes the lowest excited state in the narrow type-II GaAs-AlAs QW.

ACKNOWLEDGMENTS

The authors thank T. Hiruma, Y. Suzuki, Y. Sugiyama, and Y. Ohtake of Hamamatsu Photonics K.K. for their encouragement throughout this work, and N. Ohtani of Communications Research Laboratories for his helpful discussions. Part of this study was performed at ATR Adaptive Communications Research Laboratory with the support of the Telecommunications Advancement Organization of Japan.

APPENDIX: EXPLICIT EXPRESSIONS FOR CALCULATION OF EXCITON ENERGY

In this appendix, we present explicit expressions for calculations of exciton binding energies. Although the expressions were previously provided in Refs. 31 and 33, they are again given here for the self-contained formulation and to clarify the original modification in this paper.

The definitions and the final forms for calculation of $G(a)$, $J(a)$, and $K(a)$ are listed as follows. For relative motion of an *e-h* pair in the *z* direction, $G(a)$ is given as:

$$G(a)=\int_0^\infty 2\pi r dr\left[\left.\frac{\partial\phi_{e\text{-}h}(r,z_e-z_h)}{\partial z_e}\right|_{z_e-z_h=a}\right]^2$$
$$=\frac{2\pi\zeta^4a^2}{\lambda^2}\int_0^1 du\exp\left[-\frac{\zeta^2 a}{\lambda}\left(\frac{1}{u}+u\right)\right]\frac{1-u^2}{u(1+u^2)}, \tag{A1}$$

while $J(a)$ for the relative motion in the xy direction becomes

$$J(a)=\int_0^\infty 2\pi r dr\,\phi_{e\text{-}h}\left(\frac{\partial^2}{\partial x^2}+\frac{\partial^2}{\partial y^2}\right)\phi_{e\text{-}h}$$
$$=\pi\left(\frac{\zeta a}{\lambda}-\frac{1}{2}\right)\exp\left(-\frac{2\zeta a}{\lambda}\right)-\frac{2\pi\zeta a}{\lambda}\int_0^1 du\;\frac{\frac{1}{u^2}-1}{\frac{1}{u}+u}$$
$$\times\left[\frac{2}{\frac{1}{u}+u}+\frac{\zeta a}{\lambda}\right]\exp\left[-\frac{\zeta a}{\lambda}\left(\frac{1}{u}+u\right)\right]. \tag{A2}$$

As seen in Eq. (16) in the text, total kinetic energy for relative motion of *e-h* is given as an integral of $G(a)$ and $J(a)$ with "weight" $p(a)$ multiplied by $\hbar^2/2M^\perp$. When the effective mass mismatch between different materials is considered, the weighted spatial average of the effective mass ($\overline{m}_\alpha$) presents a simple but effective treatment. The definition of $\overline{m}_\alpha$ is given as (also seen in Ref. 25)

$$\frac{1}{\overline{m}_\alpha}=\int dz\frac{\psi_\alpha^2(z)}{m_\alpha}. \tag{A3}$$

With Eq. (A3), the weighted spatial average of the *e-h* reduced mass is defined as $1/\overline{M}^\perp=1/\overline{m}_e+1/\overline{m}_h$. The averaged effective mass introduces changes of a few percentage points to the Fermi levels.

The remaining term $K(a)$ representing the Coulomb interaction of the *e-h* pair is given as:

$$K(a)=\int_0^\infty 2\pi r dr\frac{\phi_{e\text{-}h}^2}{r}$$
$$=\pi\sqrt{1-\zeta^2}a\int_0^{(1-\zeta)/\sqrt{1-\zeta^2}}du\left(\frac{1}{u^2}-1\right)$$
$$\times\exp\left[-\frac{\sqrt{1-\zeta^2}a}{\lambda}\left(\frac{1}{u}-u\right)\right]. \tag{A4}$$

In this expression, we only consider the case of $0<\zeta<1$.

To count the dielectric mismatch in different media, we apply a rough approximation that the Coulomb energy between the electron and hole in different dielectric media is given as an average of energies in uniform media. In this approximation, the total Coulomb energy becomes

$$-\frac{e_0^2}{4\pi}\int da\;\frac{K(a)}{\overline{\epsilon}(a)}, \tag{A5}$$

where

$$\frac{1}{\overline{\epsilon}(a)}=\int dz\;\frac{\epsilon(z)+\epsilon(z+a)}{2\epsilon(z)\epsilon(z+a)}[|\psi_e(z+a)|^2|\psi_h(z)|^2$$
$$+|\psi_e(z)|^2|\psi_h(z+a)|^2] \tag{A6}$$

is an uncorrelated average of the inverse dielectric constant. It is noted that the effect of image charges is not considered here.

In the actual computations, the total energy of the 1*s* exciton must be explicitly normalized. In Refs. 31 and 33, the normalization factor $\mathcal{N}$ is defined as

$$\mathcal{N}=\int da\,p(a)F(a), \tag{A7}$$

where

$$F(a)=\int 2\pi r dr\;\;\phi_{e\text{-}h}(r,a)^2$$
$$=2\pi\int r dr\;\;\exp\left[-2\frac{\sqrt{r^2+\zeta^2a^2}}{\lambda}\right]. \tag{A8}$$

Thus, we can obtain the total energy of the 1*s* exciton per *e-h* pair as $E_{\mathrm{EXC}}/\mathcal{N}$ by using the expressions given in this appendix.

Partial derivatives of $F(a)$, $G(a)$, $J(a)$, and $K(a)$ according to the variational parameters ζ and λ are needed in the variational minimization to determine the envelope func-

tion. The derivatives are simply obtained by applying partial differentiation without any care for the order of integral and differential, because the integrals are replaced with finite sums in the practical calculation. Care is needed only for calculating $\partial K(a)/\partial\zeta$ because parameter ζ is also included in the upper integral region, as seen in the right-hand side of Eq. (A4). However, the partial differentiation is performed easily by using the relation

$$\frac{\partial I(\alpha)}{\partial\alpha}=\frac{\partial f(\alpha)}{\partial\alpha}g(f(\alpha),\alpha)+\int^{f(\alpha)}dx\,\frac{\partial g(x,\alpha)}{\partial\alpha}, \quad \text{(A9)}$$

where we define $I(\alpha)$ as follows with two functions $f(\alpha)$ and $g(x,\alpha)$, both of which are differentiable according to α,

$$I(\alpha)=\int^{f(\alpha)}dx g(x,\alpha). \quad \text{(A10)}$$

*Electronic address: taro@crl.hpk.co.jp

[1] Y. Kuramoto and H. Kamimura, J. Phys. Soc. Jpn. **37**, 716 (1974).
[2] E.A. Andryusin and A.P. Silin, Fiz. Tverd. Tela (Leningrad) **18**, 2130 (1976) [Sov. Phys. Solid State **18**, 1243 (1976)].
[3] E.A. Andryusin, Fiz. Tverd. Tela (Leningrad) **18**, 2493 (1976) [Sov. Phys. Solid State **18**, 2493 (1976)].
[4] E.A. Andryusin and A.P. Silin, Fiz. Tverd. Tela (Leningrad) **21**, 219 (1979) [Sov. Phys. Solid State **21**, 129 (1976)].
[5] S. Schmitt-Rink, C. Ell, and H. Haug, Phys. Rev. B **33**, 1183 (1986).
[6] D.A. Kleinman, Phys. Rev. B **33**, 2540 (1986).
[7] P. Hawrylak, Phys. Rev. B **39**, 6264 (1989).
[8] G.E.W. Bauer and T. Ando, Phys. Rev. B **34**, 1300 (1986).
[9] G. Tränkle, H. Leier, A. Forchel, H. Haug, C. Ell, and G. Weimann, Phys. Rev. Lett. **58**, 419 (1986).
[10] H. Kalt, J. Lumin. **60**, 262 (1994).
[11] K. Boujdaria, D. Scalbert, and C. Benoit à la Guillaume, Phys. Status Solidi B **183**, 309 (1994).
[12] W. Langbein, H. Kalt, S. Hallstein, J. Hvam, R. Nötzel, H-P. Schönherr, and K. Ploog, Superlattices Microstruct. **15**, 47 (1994).
[13] V.B. Timofeev, A.V. Larionov, M. Grassi-Alessi, M. Capizzi, and J.M. Hvam, Phys. Rev. B **61**, 8420 (2000).
[14] Q. Wu, R.D. Grober, D. Gammon, and D.S. Katzer, Phys. Status Solidi B **221**, 505 (2000).
[15] I. Shtrichman, C. Metzner, E. Ehrenfreund, D. Gershoni, K.D. Maranowski, and A.C. Gossard, Phys. Rev. B **65**, 035310 (2001).
[16] T. Ando, H. Taniyama, N. Ohtani, M. Hosoda, and M. Nakayama, IEEE J. Quantum Electron. **38**, 1372 (2002).
[17] T. Ando, H. Taniyama, N. Ohtani, M. Nakayama, and M. Hosoda, J. Appl. Phys. **94**, 4489 (2003).
[18] R.C. Miller, D.A. Kleinman, W.T. Tsang, and A.C. Gossard, Phys. Rev. B **24**, 1134 (1981).
[19] R.L. Greene, K.K. Bajaj, and D.E. Phelps, Phys. Rev. B **29**, 1807 (1984).
[20] G.D. Sanders and Y.-C. Chang, Phys. Rev. B **32**, 5517 (1985).
[21] P. Vashishta, R. K. Kalia, and K. S. Singwi, in *Electron-Hole Droplets in Semiconductors*, edited by C. D. Jeffries and L. V. Keldysh (North-Holland, Amsterdam, 1983).
[22] K.M.S.V. Bandara, D.D. Coon, O. Byungsung, Y.F. Lin, and M.H. Francombe, Appl. Phys. Lett. **53**, 1931 (1988).
[23] W.L. Bloss, J. Appl. Phys. **66**, 3639 (1989).
[24] M. Seto and M. Helm, Appl. Phys. Lett. **60**, 859 (1992).
[25] M. Helm, in *Intersubband Transitions in Quantum Wells: Physics and Device Applications I*, edited by H. C. Liu and F. Capasso (Academic Press, San Diego, 2000).
[26] See, for review, M.C. Payne, M.P. Teter, D.C. Allan, T.A. Arias, and J.D. Joannopoulos, Rev. Mod. Phys. **64**, 1045 (1992), and references therein.
[27] O. Gunnarsson and B.I. Lundqvist, Phys. Rev. B **13**, 4274 (1976).
[28] O. Gunnarsson, M. Jonson, and B.I. Lundqvist, Phys. Rev. B **20**, 3136 (1979).
[29] In Ref. 9, it is stated that the calculation of density parameters with 3D heavy-hole mass corresponds well to examinations in highly filled conditions. However, because higher states are not occupied at the density where the total EHP energy takes the minimum value, we calculate the density parameters with 2D mass. Effects of the occupation in higher states only appear in high-density regions and reduce the incline of the curves, making small corrections to the EHP energies.
[30] The band-mixing effect also produces the total shift of hole subbands. However, it is noted that the shifts of the subband levels are almost canceled in the difference between the energies of the exciton and EHP, so far as those corrections work similarly on both the exciton and EHP. Although the common changes of subband levels may produce different effects on the exciton and EHP energies, they are considered as further smaller modifications.
[31] For example, Paul Harrison, *Quantum Wells, Wires, and Dots* (John Wiley & Sons, Inc., Chichester, 2000).
[32] J. Warnock, B.T. Jonker, A. Petrou, W.C. Chou, and X. Liu, Phys. Rev. B **48**, 17 321 (1993).
[33] T. Piorek, P. Harrison, and W.E. Hagston, Phys. Rev. B **52**, 14 111 (1995).
[34] L.C. Andreani and A. Pasquarello, Phys. Rev. B **42**, 8928 (1990).
[35] Z.S. Piao, M. Nakayama, and H. Nishimura, Phys. Rev. B **53**, 1485 (1996).
[36] M. Zachau, F. Koch, G. Weimann, and W. Schlapp, Phys. Rev. B **33**, 8564 (1986).
[37] E.M. Conwell and M.O. Vassell, Phys. Rev. **166**, 797 (1968).
[38] B. Rheinlander, H. Neumann, P. Fischer, and G. Kuhn, Phys. Status Solidi B **49**, K167 (1972).
[39] F.H. Pollak, C.W. Higginbotham, and M. Cardona, J. Phys. Soc. Jpn. **21**, 20 (1966).
[40] D.E. Aspnes, S.M. Kelso, R.A. Logan, and R. Bhat, J. Appl. Phys. **60**, 754 (1986).
[41] H. C. Casey and J. K. Butler, in *Heterostructure Lasers* (Academic, New York, 1978), P. A, p. 193.
[42] *Numerical Data and Functional Relationships in Science and Technology*, edited by O. Madelung, Landolt-Börnstein, New Series, Group III, Vol. 17, Pt. a (Springer, Berlin, 1982), p. 223.
[43] The density-dependent energy of the type-II exciton is also observed experimentally in V. Negoita, D.W. Snoke, and K. Eberl, Phys. Rev. B **61**, 2779 (2000). Our calculation shows good agreement with the experimental result below the exciton density of $10^{11}1/\mathrm{cm}^2$.
[44] D.A. Kleinman, Phys. Rev. B **28**, 871 (1983).